Hydrodynamics of colloidal crystals

Jos Derksen and Willem van de Water
Physics Department, Eindhoven University of Technology, P.O. Box 513, 5600 MB Eindhoven, The Netherlands
(Received 28 December 1990)

We study the hydrodynamics of colloidal crystals in a thin-film cell using dynamic-light-scattering techniques. The measured time dependence of the fluctuating scattered light intensity reflects the characteristic frequencies of crystal modes. At variance with the theory of hydrodynamic interactions in colloidal crystals, photon-correlation functions of light scattered by longitudinal modes are nonexponential. In the long-wavelength limit, transverse modes acquire a finite damping due to the finite sample thickness. We systematically investigate this effect as a function of cell separation.

PACS number(s): 82.70.Dd, 42.25.Fx, 63.20.−e

I. INTRODUCTION

Characterizing the hydrodynamics of concentrated suspensions is an important problem of statistical physics. Its difficulty lies in the long-range character of the interaction between particles that is mediated through the fluid in which they are suspended. In a colloidal, highly deionized dispersion the suspended particles may acquire a net electric charge which causes them to order into a crystalline state [1]. Perhaps surprisingly, the hydrodynamic interaction in such an ordered state is much stronger than that in the disordered case. For example, for the sedimentation velocity of a cubic lattice of spheres, Hasimoto has shown that the correction to the single-sphere Stokes law scales with the volume fraction ϕ as $\phi^{1/3}$, whereas it is to lowest order proportional to ϕ in the disordered case [2].

The lattice dynamics of colloidal crystals presents a nice testing ground for theories of hydrodynamic interaction. The colloidal crystals that are discussed in this paper are formed of monodisperse spheres with a typical radius of $a=0.05$ μm suspended in water. The bcc-lattice parameter R_0 is typically 1 μm, so that crystallography can be done with visible light. Lattice waves are excited by Brownian forces and damped by hydrodynamic friction. The thermally excited crystal diffusively scatters light outside Bragg reflections. A judicious choice of the scattering geometry allows one to distinguish experimentally the various modes of motion of the crystal. The (complex) characteristic frequency of these modes is then accessible through analysis of the fluctuations in the scattered light intensity. It turns out that these techniques, which are analogous to those using neutron scattering in the case of atomic crystals, provide a fine probe of microhydrodynamics.

Different modes of motion in the colloidal crystal are characterized by different types of hydrodynamic interaction. For example, in longitudinal waves the relative motion of fluid and particles is largest and the friction forces are strongest. It is quite the opposite in case of transverse modes where in the long-wavelength limit the motion of the spheres and surrounding fluid is perfectly synchronized. Because the fluid is in a highly deionized state, electrodynamic effects that are associated with the motion of the counterions that surround each charged sphere and shield its Coulomb field may come into play in subtle ways.

Seminal work on the lattice dynamics of colloidal crystals was done by Hurd *et al.* [3], who studied the dispersion of lattice waves using photon-correlation spectroscopy. Based on the early work of Hasimoto [2], the same authors have also developed a theory of hydrodynamic interaction in colloidal crystals [4]. The theory involves the linear Navier-Stokes equations in the Stokes regime; retardation effects associated with fluid inertia have not yet been considered.

To prevent multiple scattering, Hurd *et al.* [3] studied crystals in a 38-μm-wide thin-film cell. It was anticipated, but not demonstrated experimentally, that such a configuration would introduce wall effects. The importance of wall interaction in the thin-film cell was illustrated by considering a very simple model of a string of spheres near a wall [4].

The theory of hydrodynamic interaction in a colloidal crystal predicts that the damping of transverse modes vanishes in the long-wavelength limit. In striking discrepancy with this prediction, Hurd *et al.* [3] found that the damping remained finite instead. This discrepancy prompted Felderhof and Jones [5] to reconsider the original hydrodynamic theory and to introduce electrodynamic effects caused by the motion of the counterions surrounding the charged spheres [6]. Felderhof and Jones were indeed able to reconcile the discrepancy between theory and the experiments of Hurd *et al.* [3]. They argued that the dipole forces due to the lag of counterions about the moving spheres caused a finite damping of transverse phonons at $q=0$.

The present paper carefully reconsiders the original experiments of Hurd *et al.* [3]. By performing a series of measurements for a range of thin-film thicknesses [27–128 μm], we show that wall effects are indeed important and cause a finite damping of shear waves in a range of q values, $q<q_0$, where q_0 increases with decreasing cell spacing. This adequately explains the finite damping

of shear waves that was found by Hurd *et al.* [3], who used a thin-film cell 38 μm wide. The widest cell (128 μm) we used exhibited a vanishing damping at the smallest q measured. These findings raise profound questions about Felderhof and Jones's theory [6] that explained the finite damping of long shear waves in terms of electrodynamic effects but did *not* consider the effect of the finite cell spacing.

The dynamics of overdamped crystal shear waves has two experimentally accessible characteristic time scales, a slow one that is determined by the interplay of crystal elasticity and hydrodynamic damping and a fast time scale that, in the limit of long wavelength, reflects the damping of pure hydrodynamic shear waves. The ratio of these time scales is $O(10^{-3})$. We measured correlation functions on both time scales and propose a tentative explanation of these results in terms of the discrete character of hydrodynamic modes with wave vector perpendicular to the cell walls.

Dispersion functions of Brownian crystal waves are generally extracted from a series of correlation spectra measured in various scattering configurations. We will argue that the shape of those correlation functions forms an important body of qualitative information. Namely, only if the characteristic frequencies of crystal dynamics are spaced far enough apart on the imaginary axis, will the correlation function exhibit simple exponential behavior on its slowest time scale. A severe drawback of the thin-film configuration in studying the shape of correlation functions is the large and varying fraction of the incident beam that scatters off glass surfaces. This reflected light causes an unknown heterodyne contribution to the correlation function which affects its shape and renders its interpretation ambiguous. We have cured this problem by designing a mechanically flexible heterodyne spectrometer employing single-mode optical fibers. This enabled us to precisely measure the shape of correlation functions and compare it to theory, that predicts simple-exponential correlation functions. It will turn out that, quite contrary to this prediction, correlation functions of light scattered by longitudinal modes are *not* simple exponential.

Colloidal crystals exhibit phenomena that have analogs in simple liquids and molecular solids. Phase transitions [7] and nonequilibrium phenomena [8] have been studied using visible light. Of particular interest are the measurements of dynamic structure factors that revealed the presence of a hexatic phase in two-dimensional colloidal crystals [9]. The macroscopic, rheological properties of strongly deionized fluids have been studied for many years [10].

In Sec. II, we will summarize the theory of hydrodynamic interactions in a colloidal crystal and discuss the relevance of electrodynamic effects [6]. We also show in what manner the spectrum of characteristic frequencies is folded into measured photon-correlation spectra. Our treatment lacks detail, detail that is dealt with extensively in the original treatments of Hurd *et al.* [4] and Felderhof and Jones [5,6]. In Sec. III the experimental setup is described and the techniques to measure heterodyne correlation functions of light scattered by crystal waves are detailed. The results are discussed in Sec. IV, where we present correlation spectra and dispersion functions of longitudinal and transverse phonons.

II. CRYSTAL DYNAMICS AND SCATTERED-LIGHT CORRELATION FUNCTIONS

A. Crystal hydrodynamics

The physics of colloidal crystals embodies an intricate interplay between well-known concepts of solid-state physics and the (hydro)dynamics of colloids. Because our prime interest is in the latter, we would like to unravel both aspects and delineate their contribution to the quantities of experimental interest, i.e., the characteristic frequencies of the crystal. The fundamental building blocks of a theory of colloidal crystal dynamics are the linear Navier-Stokes equations for incompressible and low-Reynolds-number flow

$$-i\omega\rho\mathbf{v}=\eta\nabla^2\mathbf{v}-\nabla p+\mathbf{f}\ ,\qquad \nabla\cdot\mathbf{v}=0\ , \tag{1}$$

where the frequency notation has been used $[\mathbf{v}(t)=\mathbf{v}(\omega)\exp(-i\omega t)]$, and the Langevin equation for the motion of a sphere with index j

$$-i\omega m\mathbf{u}_j=\mathbf{F}_j-\mathbf{f}_j+\mathbf{X}_j\ . \tag{2}$$

In the equations of motion $\mathbf{v}(\mathbf{r},\omega)$ is the velocity field of the fluid with pressure $p(\mathbf{r},\omega)$, density ρ, and dynamic viscosity η, and $\mathbf{u}_j$ is the velocity of sphere j. The ensemble of spheres exerts a force density $\mathbf{f}$ on the fluid that is assumed a sum of point forces concentrated at the lattice sites $\mathbf{R}_j$, $\mathbf{f}(\mathbf{r},t)=\sum_j \mathbf{f}_j(t)\delta(\mathbf{r}-\mathbf{R}_j)$.

The associated reaction force on each of the spheres is represented by the term $-\mathbf{f}_j$ in the equation of motion of the spheres, Eq. (2). Each of the spheres is bound into the crystal lattice by a short-range electrostatic force $\mathbf{F}_j$ between it and its nearest and next-nearest neighbors. The stochastic force $\mathbf{X}_j$ that drives Brownian lattice vibrations is assumed white noise and uncorrelated at different lattice sites.

In the harmonic approximation the electrostatic forces define the well-known crystal elastic tensor D

$$\mathbf{F}_j=-\sum_{\substack{k\\k\neq j}} D(\mathbf{R}_j-\mathbf{R}_k)(\mathbf{s}_j-\mathbf{s}_k)\ , \tag{3}$$

where $\mathbf{s}_j$ is the displacement of a sphere from its equilibrium position $\mathbf{R}_j$. A description in terms of linear hydrodynamics implies a linear relationship between the flow field at location $\mathbf{r}$ and the point forces $\mathbf{f}_j$ at the lattice sites that induce it.

$$v(\mathbf{r},\omega)=\sum_{\mathbf{k}} T(\mathbf{r}-\mathbf{R}_{\mathbf{k}},\omega)\mathbf{f}_k(\omega)\ . \tag{4}$$

In the zero-frequency limit, the tensor T equals the well-known Oseen tensor [11].

The unknown forces $\mathbf{f}_j$ can be eliminated from Eqs. (1) and (2) through prescription of the boundary condition on the sphere surface. The condition that the particle ve-

locity be equal to the fluid velocity averaged over the sphere surface was first proposed by Burgers [12]

$$-i\omega \mathbf{s}_j = \sum_{\mathbf{k}} \langle T(\mathbf{r}-\mathbf{R}_{\mathbf{k}},\omega)\rangle_{\sigma_j} \mathbf{f}_{\mathbf{k}} , \tag{5}$$

where $\langle\ \rangle_{\sigma_j}$ denotes an average over the spherical surface of particle j.

Equations (2) and (5) embody the essential physics of hydrodynamic interactions in colloidal crystals. They are in the form of infinite-dimensional matrix equations. As is well known from solid-state theory [13], these equations can be turned into ordinary three-dimensional matrix equations for each crystal wave vector $\mathbf{q}$ by expanding $\mathbf{s}$, $\mathbf{X}$, D and $\langle T\rangle_{\sigma_j}$ in normal modes, for example $\mathbf{s}_j = \sum_q \mathbf{a}_q e^{i\mathbf{q}\cdot\mathbf{R}_j}$, and $D_{ij} = \sum_q D(\mathbf{q},\omega) e^{i\mathbf{q}\cdot(\mathbf{R}_i-\mathbf{R}_j)}$. This leads to the equation of motion

$$M\mathbf{a}_q = \frac{1}{m}\mathbf{X}_q ,$$

with (6)

$$M(\mathbf{q},\omega) = -\omega^2 I + \frac{1}{m}D(\mathbf{q}) - \frac{i\omega}{m}T^{-1}(\mathbf{q},\omega) ,$$

where $D(\mathbf{q})$ and $T(\mathbf{q},\omega)$ are the lattice transforms of the potential and hydrodynamic friction matrices, respectively, and I is the unit tensor.

While the imaginary part of the friction matrix T can be expressed as an effective mass $\mu(\mathbf{q})$ multiplying the inertia term $-\omega^2 I$ in Eq. (6), its real part is

$$T(\mathbf{q},\omega) = S(\mathbf{q}) + Y(\mathbf{q},\omega) , \tag{7}$$

with

$$Y(\mathbf{q},\omega) = \frac{1}{v_c \eta}\frac{q^2}{q^4-(\omega\rho/\eta)^2}\frac{\sin(qa)}{qa}(I-\hat{\mathbf{q}}\hat{\mathbf{q}}) , \tag{8}$$

and

$$S(\mathbf{q}) = \frac{1}{6\pi\eta a}[I-\kappa(\mathbf{q})\phi^{1/3}] ,$$

where v_c is the volume of the unit bcc cell ($v_c = R_0^3/2$), and a is the radius of a sphere. The matrix Y embodies the shear friction; it vanishes for longitudinal waves. The matrix S reflects the friction between spheres and fluid; it is gauged by the Stokes friction ($S^{-1} \cong 6\pi\eta a$), and contains the matrix $\kappa(\mathbf{q})$ that has been tabulated for several values of $\mathbf{q}$ by Hurd *et al.* [4]. The derivation of the lattice sum S is discussed in detail in Hasimoto's treatment of the sedimentation of regular arrays of spheres.

The normal modes of the crystal are defined through the matrix N_q that diagonalizes $M(\mathbf{q},\omega)$. For the special choices of $\mathbf{q}$ that are considered here, the normal modes are very simple. For $\mathbf{q}$ in the [100] direction they fall along the elementary axes of the simple cubic reciprocal lattice, whereas for $\mathbf{q}$ in the [110] direction the longitudinal mode has the components $(1/\sqrt{2}, 1/\sqrt{2}, 0)$.

The zeros of the characteristic equation, $|M(\mathbf{q},\omega)| = 0$, are the key quantities of interest in a light-scattering experiment. As will be explained in Sec. II B, these zeros determine the time dependence of the scattered-light intensity. The characteristic frequencies of longitudinal and transverse modes are determined by the appropriate element of M

$$M^{L,T}(\mathbf{q},\omega) = 0 ,$$

or explicitly

$$\mu_q^{L,T}\omega^2 - (\omega_q^{L,T})^2 + i\omega\lambda_q^{L,T}(\omega) = 0 . \tag{9}$$

For the colloidal crystals studied so far, the zeros of the characteristic equation are almost always purely imaginary and, consequently, the correlation function of light scattered by crystal waves is a sum of decaying exponentials with the characteristic frequencies as decay rates. It is a well-known fact that such measured functions can only be interpreted unequivocally if these characteristic frequencies are spaced far enough apart on the imaginary axis [14].

For longitudinal waves in the [100] direction, Eq. (9) has two imaginary roots

$$\omega_{q1}^L = -i\lambda_q^L/\mu_q^L , \quad \omega_{q2}^L = -i(\omega_q^L)^2/\lambda_q^L .$$

In dilute crystals the friction λ_q^L equals the Stokes friction, $\lambda_q^L \cong 6\pi\eta a/m$. The first zero ω_{q1}^L, therefore, is associated with the rapid decay of the velocity autocorrelation of Brownian motion, $1/|\omega_{q1}^L| = O(10^{-8}$ s). The second zero reflects the interplay between crystal elasticity and hydrodynamic friction; it is much smaller than the first, $1/|\omega_{q2}^L| = O(10^{-3}$ s). Because the crystal elastic frequency $\omega_q^L = \sqrt{D/m}$ vanishes as $\omega_q^L \simeq q$ for large wavelengths, ω_{q2}^L approaches zero at the zone center.

In the case of transverse waves the characteristic equation is *third order* with three widely separated zeros on the imaginary axis.

$$\omega_{q1}^T \cong -i\frac{6\pi\eta a}{m} ,$$

$$\omega_{q2}^T = -i\lambda_q^T/\mu_q^T ,$$

$$\omega_{q3}^T = -i(\omega_q^T)^2/\lambda_q^T .$$

The first root is again the rapid decay of the Brownian velocity autocorrelation. Contrary to that of longitudinal modes, the damping λ_q^T of transverse waves vanishes at long wavelengths where the particles and spheres move in concert. There, the relaxation rate reduces to that of pure hydrodynamic shear waves, $\omega_{q2}^T = -i\eta q^2/\rho$, and the third zero ω_{q3}^T remains finite at the zone center. In general $\omega_{q2}^T \gg \omega_{q3}^T$, except at very small values of q where transverse waves may even turn from overdamped to propagating [$\lambda_q^T < 2\omega_q^T(\mu_q^T)^{1/2}$].

Scattered-light correlation functions will be dominated by their slowest decaying component. In the framework of a purely hydrodynamic theory this slowest component has a time constant $1/|\omega_{q3}^T|$ or $1/|\omega_{q2}^L|$, for transversal and longitudinal modes, respectively. An important conclusion then is that these time constants are well separated from other decay constants, except perhaps near $q = 0$.

Felderhof and Jones [6] have criticized such a purely hydrodynamic theory, noticing the importance of ion dynamics in colloidal crystals. In the static situation each

sphere with charge Ze at lattice site $\mathbf{R}_j$ is surrounded by its Debye cloud which evokes a screened electrostatic potential

$$\Psi(\mathbf{r})=Ze\frac{e^{-\kappa|\mathbf{r}-\mathbf{R}_j|}}{4\pi\epsilon|\mathbf{r}-\mathbf{R}_j|}\ , \tag{10}$$

where κ is the inverse Debye length, $\kappa^2=n_0z^2e^2/\epsilon k_BT$, n_0 the density of counterions with charge ze, k_B the Boltzmann constant, and ϵ the dielectric constant of the fluid. When the particles oscillate about their equilibrium positions, the cloud of counterions around each sphere is perturbed both due to the motion of the particle itself and due to long-range interactions with induced dipoles associated with all other particles that have moved from their equilibrium positions. Ignoring the convection of ions by the flowing solvent, Felderhof and Jones describe the motion of the sea of counterions by a generalized diffusion equation. Accordingly, the electrodynamic force on particle j can be split into two parts, $\mathbf{H}_j$ and $\mathbf{G}_j$, that enter the right-hand side of the Langevin equation [Eq. (2)]. The contribution $\mathbf{G}_j$ is the friction force on sphere j due to deformation of its own Debye cloud by the particle itself and the term $\mathbf{H}_j$ embodies long-range dipole interactions. The self-force $\mathbf{G}_j$ is proportional to the particle velocity $\mathbf{u}_j$ and would also be present in very dilute, random colloids. In the frequency notation

$$\mathbf{G}_j(\omega)=\frac{\kappa^2}{12\pi\epsilon}(\kappa-\lambda)Z^2e^2\mathbf{s}_j\equiv i\omega\zeta_e(\omega)\mathbf{s}_j\ , \tag{11}$$

where $\lambda^2=\kappa^2-i\omega/D^i$, with D^i the ion-diffusion constant. The frequency-dependent dipole force on particle j is

$$\mathbf{H}_j(\mathbf{r},\omega)=-i\omega\frac{Z^2e^2}{4\pi D^i\lambda^2\epsilon}\sum_{i\ (\neq j)}U(\mathbf{R}_i-\mathbf{R}_j)\cdot\mathbf{s}_j\ , \tag{12}$$

where $U(\mathbf{r})$ is the dipole tensor, $U(\mathbf{r})=(3\hat{\mathbf{r}}\hat{\mathbf{r}}-I)/r^3$.

Both electrodynamic effects, the ion-diffusion self-force and the induced dipole force, give rise to extra contributions in the equation of motion of a longitudinally polarized lattice wave. The enhanced equation is similar to Eq. (6), except that the hydrodynamic friction term $S^{-1}(\mathbf{q})$ needs be replaced by $S^{-1}(\mathbf{q})+H(\mathbf{q},\omega)+\zeta_e(\omega)I$, where $H(\mathbf{q},\omega)$ is the lattice transform of the dipole force. The frequency dependence of $H(\mathbf{q},\omega)$ introduces a new zero of the characteristic equation that is related to the time a counterion needs to diffuse over a Debye length, $\omega_k^L=-iD^i\kappa^2$. For Debye lengths of 0.3 μm, this characteristic time is approximately 10 μs. It would be intermediate between the fastest hydrodynamic time scale, that is the velocity autocorrelation time, and the next fastest, that is the decay time of hydrodynamic shear fluctuations. Ionic effects should be manifest in correlation functions measured on this time scale, especially in the case of longitudinal waves where the relative motion of spheres and fluid is strongest.

The damping of transverse waves can in the long-wavelength limit be approximated similarly to that in the pure hydrodynamic case, $\lambda_q^T\cong[(Ze/D^i\lambda^2)U_{yy}(q)+\zeta_e(\omega)]/m$. In striking contrast with the case with only hydrodynamic interactions, the damping now remains finite at infinite wavelengths

$$\lambda_q^T\cong\frac{Z^2e^2\kappa}{3m\epsilon D^i}\left[\frac{1}{8\pi}-\frac{2}{\kappa^3R_0{}^3}\right]\ . \tag{13}$$

A peculiar consequence of this description of electrodynamics is that the damping of long shear waves may turn negative if the Debye length becomes larger than a critical value $\kappa R_0\lesssim 3.7$. Although it is not clear whether larger Debye lengths actually lead to an instability of shear waves, a crude estimate of the Debye length in our samples ($\kappa R_0\cong 10$, see Sec. IV) actually satisfies this criterion.

The values of the characteristic frequencies reflect the elementary physical processes that characterize colloidal dynamics: elastic interaction, friction between the spheres and the fluid, internal friction in the fluid alone, and, possibly, the relaxation of ion clouds through diffusion. The analysis of the experiment is simplified considerably if these time scales are very different. We conclude that they actually are, with the possible exception of the ion-diffusion time scale which may become of the same order as the relaxation time of hydrodynamic shear modes.

B. Scattered-light correlation function

In the case of particle excursions $\mathbf{s}_j$ that are small with respect to the inverse wave vector of scattered light, $\mathbf{k}\cdot\mathbf{s}_j\ll 1$, the normalized scattered electric field correlation function is

$$g_1(k,\tau)=\langle E(0)E^*(\tau)\rangle/\langle EE^*\rangle$$
$$\simeq\left[\frac{8\pi^3}{v_c}\right]^2\sum_l\left[|P(\mathbf{k}-\mathbf{K}_l)|^2\left[1-\sum_q\sum_\beta C_q^\beta\sum_i(\mathbf{k}_iN_q^{i\beta})^2\rho_q^\beta(0)\right]+\sum_q|P(\mathbf{k}-\mathbf{q}-\mathbf{K}_l)|^2\sum_\beta C_q^\beta\sum_i(k_iN_q^{i\beta})^2\rho_q^\beta(\tau)\right]\ , \tag{14}$$

where the constant $C_q^\beta=2\lambda_q^\beta k_BT/m$ is a reflection of the thermal equilibrium between excited lattice waves and their environment. The time dependence of the correlation function is embodied by the function $\rho_q^\beta(\tau)$ that is determined by the characteristic frequencies of the crystal

$$\rho_q^\beta(\tau)=\int d\omega\frac{e^{-i\omega\tau}}{[(\omega_q^\beta)^2-\mu_q^\beta\omega^2-i\omega\lambda_q^\beta][(\omega_q^\beta)^2-\mu_q^\beta\omega^2+i\omega\lambda_q^\beta]}\ . \tag{15}$$

The first term in the right-hand side of Eq. (14) describes Bragg reflections. These are modulated in scattering space by the profile function $P(\mathbf{k})$, that is defined through the lattice transform of the incident field distribution over the scattering volume,

$$\sum_j E_0(\mathbf{R}_j)\exp(i\mathbf{k}\cdot\mathbf{R}_j)=\sum_l P(\mathbf{k}-\mathbf{K}_l)\ .$$

Because the linear size of the scattering volume is large with respect to the wavelength of light, the function $P(\mathbf{k})$ will be sharply peaked in the origin.

Diffuse scattering outside Bragg reflections is contained in the second term of Eq. (14). The wave vector of thermally excited lattice waves can be selected experimentally as the difference between the scattering vector and the nearest reciprocal lattice point. The experiment can also be arranged such that a single polarization direction β is selected. If the particle excursions are no longer small, this selectivity fails and the correlation function contains a contribution of all crystal wave vectors simultaneously. Scattered-light correlation functions will then in general be nonexponential.

The integration in Eq. (15) can be closed in the complex plane, with for a frequency-independent damping λ_q^β the result

$$\rho_q^\beta(\tau)\simeq\frac{\pi}{\lambda_q^\beta\mu_q^\beta(\omega_1-\omega_2)}\left[\frac{e^{-i\omega_1\tau}}{\omega_1}-\frac{e^{-i\omega_2\tau}}{\omega_2}\right], \qquad (16)$$

where $\omega_{1,2},\omega_1>\omega_2$, are the zeros of the second-order characteristic equation. Similarly, when there are more than two characteristic (imaginary) frequencies, the correlation function is an alternating sum of exponentials, each term approximately weighted by its associated decay time. This observation provides valuable guidance for the experimental detection of fast relaxation modes because it implies that the signal-to-noise ratio must be increased when detecting physical processes with smaller time scales.

If the scattered field has Gaussian statistics, the electric field correlation function is related to the experimentally more easily accessible intensity correlation function $g_2(\mathbf{k},\tau)$ through the Siegert relation $g_2=1+g_1^2$ [15]. The validity of this relation under the present circumstances has been questioned because light scattered by an orderly medium would not *a priori* have Gaussian statistics [16]. However, the excursions $\mathbf{s}_j$ of harmonically bound particles are proportional to the stochastic driving forces $\mathbf{X}_j$, whereas for small $\mathbf{s}_j$, $\mathbf{k}\cdot\mathbf{s}_j\ll 1$, there is a linear relation between the scattered electric field and $\mathbf{s}_j$. The statistical properties of the scattered electric field are therefore inherited from the Brownian forces that are Gaussian. Outside Bragg reflections the scattered field is Gaussian and the Siegert relation applies. In summary, both the Gaussian statistics of the scattered light and the crystal-wave-vector selectivity of measured correlation functions are only guaranteed if particle excursions remain small. We will, therefore, assess the validity of the assumption of small particle excursions by experimental tests of both the statistics of scattered light and the shape of correlation functions.

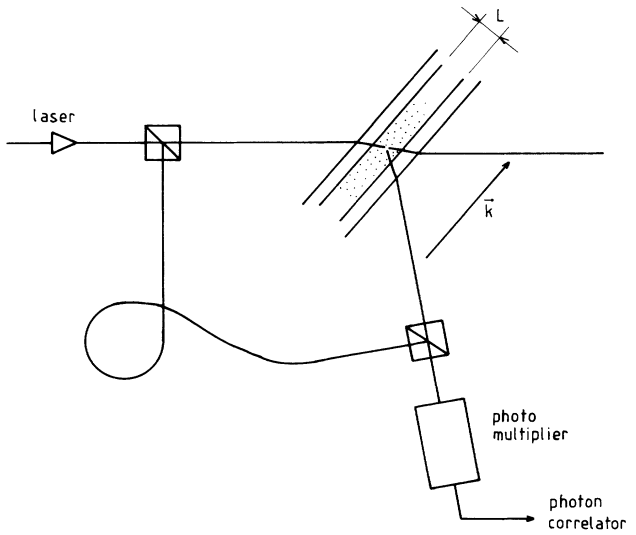

FIG. 1. Schematic view of the experiment for measuring colloidal crystal dynamics. The crystals are grown in a thin-film cell. Scattered light is detected with help of a photomultiplier. The scattered light may be mixed on the surface of the detector with a reference beam that is guided through an optical fiber.

III. EXPERIMENT

Figure 1 gives a schematic overview of the experimental setup. The colloidal crystal is contained in a thin-film cell with adjustable thickness (20–400 μm). It is illuminated by light from a HeNe laser (wavelength 633 nm) and the scattered light is mixed with a fraction of the incident beam that is transported through an optical fiber. The thin-film concept has been adopted from Hurd *et al.* [3]; however, the optical setup is rather different.

The thin-film cell shown in Fig. 2 was manufactured from optically flat quartz windows that were separated by an *O* ring that served both to seal the colloid reservoir and as a spring to allow cell spacing adjustment. In one window an annular groove was machined with three radi-

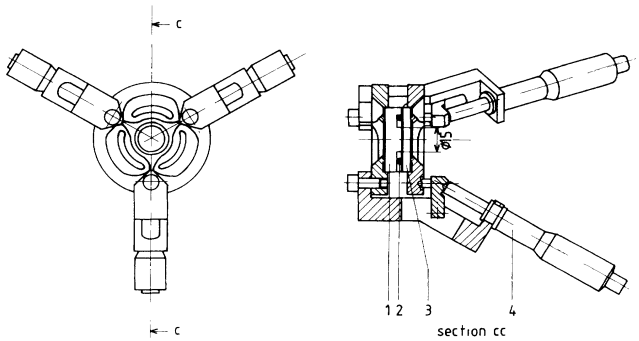

FIG. 2. Schematic view of the thin-film cell. The two quartz windows (1) and (3) are held apart by an *O* ring (2). The three micrometer screws (4) to adjust the cell separation are placed under an angle of 30° to facilitate access of the incident laser beam. Three windows for interferometric measurement of cell separation surround the central 15 mm diameter thin-film region.

al filling channels. This groove held the *O*-ring and formed the reservoir for ion-exchange resin particles. The diameter of the actual thin film was 15 mm. Three differential micrometers with a pitch of 50 μm were used to adjust the cell separation. They were mounted under an angle to facilitate access of the incident laser beam at large scattering angles. The three windows outside the *O*-ring perimeter are used for interferometric measurement of the cell spacing that could be adjusted with an accuracy of 1 μm.

The thin-film cell virtually eliminates multiple scattering; for crystals formed of polystyrene spheres (radius $a=0.053$ μm) in water with a typical lattice parameter of $R_0=0.8$ μm the optical mean free path is 5 mm. However, scattering of the incident beam off cell surfaces and intense flares due to other reflections in the cell causes the detection optics to simultaneously accept direct light and light scattered from the crystal. This leads to an unknown heterodyne component of the measured intensity correlation function that decays with twice the ordinary homodyne decay time. Although the strength of this heterodyne component depends on the scattering geometry, it is impossible to control and leads to an ambiguous interpretation of measured correlation functions.

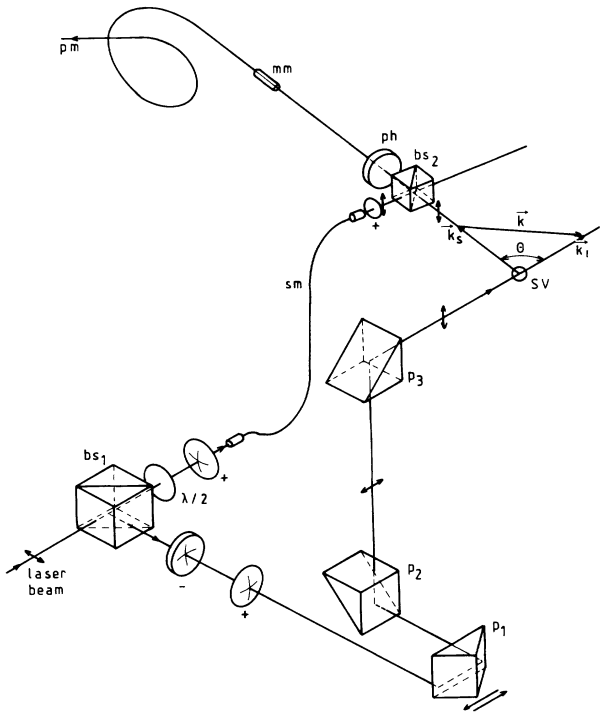

FIG. 3. Schematic view of the complete optical setup. A horizontally polarized beam emerges from a HeNe laser. A local oscillator is divided off in the beamsplitter bs_1 and guided to the detector through a single-mode optical fiber *sm*. The right-angle prisms p_1, p_2, and p_3 transport the incident beam (wave vector $\mathbf{k}_i$) to the scattering cell; the vertical translation over the thin film is achieved by horizontally translating p_1. In the detector the scattered beam (wave vector $\mathbf{k}_s$) is merged with the local oscillator in a beamsplitter bs_2. The mixed light passes a pinhole *ph* and is transported through a multimode fiber to the photomultiplier.

We have sought to cure this problem by overwhelming possible reflected light with a strong local oscillator so that always a heterodyne correlation function was measured. The use of heterodyne scattering in our experiment required an extremely stable mechanical setup that should at the same time be flexible enough to realize a large variety of scattering geometries. These seemingly contradictory requirements were satisfied by using an optical fiber to transport the local oscillator beam. The resulting optical setup is detailed in Fig. 3.

The scattered light was mixed with a fraction of the incident beam that was transported through a polarization-preserving monomode optical fiber with a core diameter of 4 μm (Newport F-SPA). The scattering geometry was defined through pinholes in the light collecting optics. The coherent mixture of scattered and local oscillator light was transported through a multimode optical fiber to a cooled photomultiplier. The photopulses were amplified, discriminated and subsequently time correlated in a digital photon correlation (ALV-3000).

The crystalline samples were prepared in quartz cuvettes by diluting monodisperse latex in clean, filtered (0.2 μm pore size) and deionized water. After adding an ample quantity of mixed-bed ion-exchange resin (Amberlite IRN-150) and stirring, the colloid crystalized spontaneously. The cell-quartz windows were cleaned with water and soap and with warm sulfochromic acid. Thereafter they were extensively rinsed with clean water. The silicon *O* ring was cleaned in an ultrasonic bath and in boiling water. The lattice parameter of the bcc crystals ranged from 0.80 to 0.74 μm; it was stable during the measurement of a dispersion curve. Single crystals with a typical size of a few mm that filled the cell gap could easily be identified in white light. The diffraction-limited angular size of the Bragg reflections was consistent with the diameter (60 μm) of the laser beam in the cell. Because the lattice parameter is relatively small, the largest angle that could be used as a starting point for the measurement of a dispersion function was a [110] Bragg reflection. The stability of the crystal was checked from the quality of this reflection when, after measuring a series of correlation functions in different scattering geometries, the cell was rotated back to its initial orientation. It appeared that this stability, especially the orientation change of the crystal with respect to an axis normal to the cell, depended on the cell width. The stability was greatest at the smallest cell separations.

In this paper we present measured dispersion functions of [100] and [110] modes only. Figure 4 illustrates the measurement of pure longitudinal waves in the [110] direction. Let us assume the incident and scattered wave vector to be in the horizontal plane. The bcc crystal has its most densely packed plane [the (110) plane] parallel to the cell walls. The cell is then rotated around a vertical axis and around an axis normal to the cell walls until the [110] Bragg reflection is observed in the horizontal plane. Further rotation of the cell over an angle θ and of the detector over an angle 2θ around a vertical axis leads to a situation where the scattering wave vector $\mathbf{k}$ and the

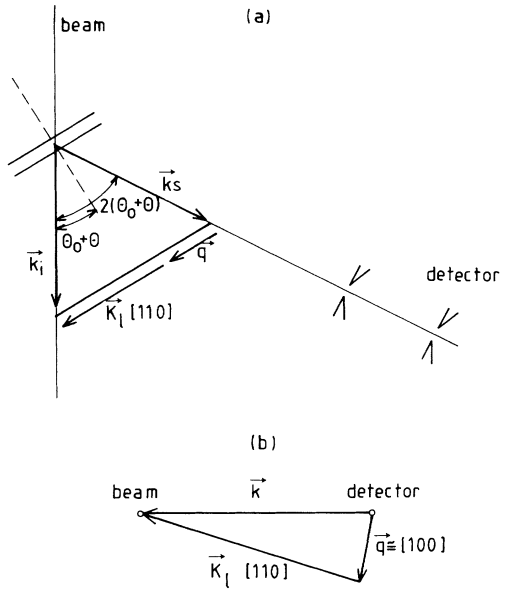

FIG. 4. (a) Scattering configuration for detecting longitudinal modes with wave vector **q** in the [110] direction. The angles θ_0 correspond to the setting with $\mathbf{q}=0$. (b) Frontal view of the scattering configuration for detecting transverse modes with **q** in the [100] direction.

wave vector **q** of crystal waves are parallel and only the longitudinal mode is detected.

The detection of pure transverse waves in symmetry directions of the crystal is not possible with a single-beam, single detector setup and one is necessarily left with the measurement of a mode mixture [17]. Such a mixture is impossible to unravel experimentally because the weights of its components in the correlation function depend upon the characteristic frequencies. Hurd *et al.* [3] present a transverse mode dispersion curve which was deduced from a mixed-mode measurement with help of a theoretical model that was fitted to a measured longitudinal dispersion curve. For relatively small wave vectors, however, the transverse mode dominates the correlation function of a mixed-mode measurement. The starting point of measuring the dispersion of [100] phonons is again a [110] Bragg reflection ($\mathbf{q}=0$ in Fig. 4). Further rotation of the cell over an angle φ around an axis normal to the cell surfaces leaves us with $k^T[=\sum_i(k_i N_{\mathbf{q}}^{iT})]=k\cos\varphi/2$ and $k^L=k\sin\varphi/2$ so that for angles $\varphi<20°$, $(k^L)^2<0.05(k^T)^2$. The weights of the transverse and longitudinal components in the correlation function are $(k^T)^2/(\omega_q^T)^2$ and $(k^L)^2/(\omega_q^L)^2$, respectively. For the range of q values of interest the crystal elastic frequencies are of the same order of magnitude.

IV. RESULTS

In order to understand ionic friction in a highly deionized fluid similar to that from which our crystals were grown we will first present the result of an experiment on more dilute random dispersions. Next we will discuss the results of an experiment that was aimed at establishing the statistical character of light scattered diffusively off colloidal crystals. Finally we will present a series of measurements both of the correlation functions and dispersion curves of longitudinal and transverse waves and show the influence of the finite thickness of the crystal.

The two parameters that characterize electric interactions in our fluid are the Debye length κ^{-1} and the surface charge Z of each sphere. The concentration of counterions n_0, and consequently the Debye length, can be inferred from the conductivity of the fluid, whereas the surface charge Z follows from an electrophoresis experiment. The present design of our thin-film cell prevents an *in situ* measurement of these parameters. However, if we assume the fluid to be highly deionized it follows that $nZ=n_0 z$. A measurement of the diffusion constant in a disordered deionized fluid contained in the thin-film cell can then be used to indirectly measure Z and κ.

According to Eq. (12), the friction of a charged sphere would be increased by

$$\zeta_e(\omega=0)=\frac{\kappa Z^2 e^2}{24\pi D^i \epsilon} \tag{17}$$

due to the ions in the surrounding Debye sphere that need be dragged along. The expression in Eq. (20) is also an approximation to a theory by Ohshima, Healy, and White [18]. We have measured the diffusion constant in a dilute solution of polystyrene spheres ($a=0.099$ μm, number concentration $n=7\times10^{16}$ m^{-3}) in water. The sample, contained in the thin-film cell, was kept in a highly deionized state by the presence of ion-exchange resin. Heterodyne photon-correlation functions were measured over a range of scattering angles. The effect of particle interactions was minimized by keeping the scattering vector larger than the characteristic wave number of the suspension ($2\pi n^{1/3}\cong 2.6\times10^6$ m^{-1}). The measured correlation functions could be represented well by single exponentials and diffusion constants were computed from their decay rates. Figure 5 shows the diffusion constant as a function of wave vector **k**, both for

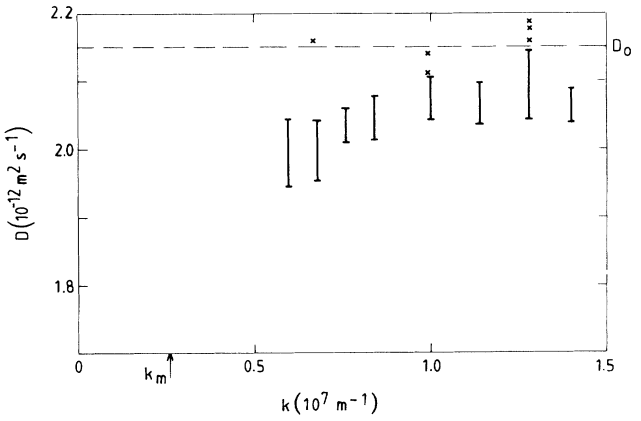

FIG. 5. Vertical error bars: measured diffusion constant as a function of the length of the scattering vector **k** for $a=0.099$ μm spheres with number density 7×10^6 m^{-3} in deionized water of $T=20$°C. Crosses: measured diffusion constant in distilled water. Dashed line: the Stokes diffusion constant $k_B T/6\pi\eta a$. K_m is the characteristic wave number of the suspension and points to the value $2\pi n^{1/3}$.

the highly deionized dispersion as well as for a solution of the same polystyrene spheres in distilled water. The diffusion constant in the deionized fluid appears to be (4±2)% smaller than that measured in the absence of ionic friction. It is consistent with the following estimates: $Z \cong 1400$, $\kappa a \cong 0.14$.

Although the results of these experiments are only qualitative, we believe that the above constants characterizing our working fluid are indicative for those in the case of our experiments on colloidal crystals. If we assume the counterion density to be scalable by the particle concentration, the Debye length in the $R_0 = 1.8$ μm crystal should be approximately $\kappa^{-1} \cong 0.2$ μm, or $\kappa R_0 \cong 10$.

Information about the statistics of scattered light was obtained from a comparison of heterodyne and homodyne correlation functions of light that was scattered by longitudinal crystal waves with (reduced) wave vector Q $(=qR_0\sqrt{2}/4\pi)=0.14$ in the [110] direction. The crystal was formed out of $a=0.099$ μm radius spheres and had an $R_0=1.8$ μm lattice parameter; it was contained in a cell with spacing $L=43$ μm. In the heterodyne measurement, which detects the second moment of the electric-field distribution, a local oscillator was mixed with the scattered light with an intensity ratio of about 50. The homodyne setup, in which the fourth moment of the field distribution is measured, was arranged such as to eliminate reflected light as well as possible. The measured heterodyne correlation function $G_{\rm het}$ was used to form the functional

$$G(\tau)=c_1+c_2G_{\rm het}(\tau)+c_3[G_{\rm het}(\tau)]^2 ,$$

where the constants $c_{1,2,3}$ were adjusted to minimize the squared difference between $G(\tau)$ and $G_{\rm hom}(\tau)$ with the result $c_1=0.0016$, $c_2=0.34$, and $c_3=0.65$. The quality of the fit in Fig. 6(a) is demonstrated in Fig. 6(b) that shows the residue $G(\tau)-G_{\rm hom}(\tau)$. It is consistent with the assumption of Gaussian statistics of scattered light. The magnitude of the residues $G(\tau)-G_{\rm hom}(\tau)$ is also consistent with the ratio of local oscillator to scattered light intensity. The nonvanishing constant c_2 indicates that the homodyne measurement was not pure due to the unavoidable presence of optical flares. This precisely prompted us to perform subsequent measurements using the heterodyne scattering setup.

Figure 7 shows a correlation function $G_1^L(\mathbf{q},\tau)$ of light scattered by longitudinal waves with wave vector $Q=0.11$ in the [110] direction. The crystal was formed out of 0.053 μm radius spheres and had a 0.8 μm lattice parameter; the cell spacing was 36 μm. We have attempted to represent $G_1^L(\mathbf{q},\tau)$ by a single exponential, $G_1^L=c_1e^{-\Gamma\tau}+c_2$, and have determined $c_{1,2}$ and Γ in a least-squares procedure over the time delay interval $[0,5\Gamma^{-1}]$. As is evident from the quality of the fit, longitudinal correlation functions are *not* simple exponentials. We would like to emphasize that this observation is at variance with the hydrodynamic theory that predicts a slowest decaying component of the correlation function whose decay rate is well separated from that of other components.

To approximately account for this nonexponentiality in a quite arbitrary fashion we have sought to represent G_1^L by $G_1^L=c_1(1+k_2\tau^2)e^{-\Gamma\tau}+c_2$, where the value of the second cumulant k_2 and the constants $c_{1,2}$ and Γ were determined in a least-squares procedure over the time interval $[0,5\Gamma^{-1}]$. This allowed us to extract the longitudinal dispersion function shown in Fig. 8 from a series of

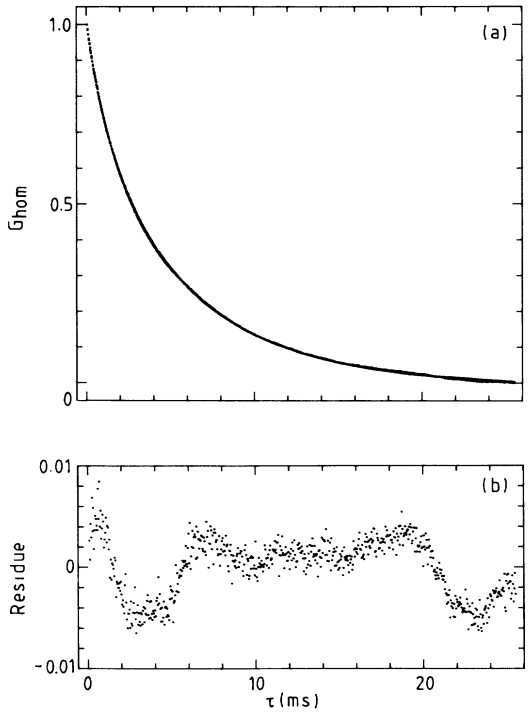

FIG. 6. (a) Homodyne correlation function $G_{\rm hom}$ of light scattered by a longitudinal crystal wave shown overlayed with a functional of the measured heterodyne correlation function $G=c_1+c_2G_{\rm het}(\tau)+c_3[G_{\rm het}(\tau)]^2$, with $c_1=0.001\,64$, $c_2=0.34$, and $c_3=0.65$. The crystal wave has $Q=0.14$ in the [110] direction. (b) Difference $G_{\rm hom}(\tau)-G(\tau)$.

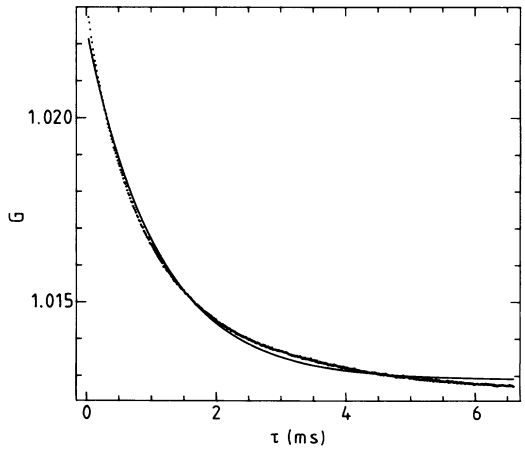

FIG. 7. Dots: measured correlation function G of light scattered by a longitudinal wave with a reduced wave vector $Q=q\sqrt{2}R_0/4\pi=0.11$ in the [110] direction. Line: fit of $G=c_1\exp(-\Gamma\tau)+c_2$, with $\Gamma=917$ Hz, $c_1=9.5\times10^{-3}$, and $c_2=1.013$.

measurements at different q. Some points taken at the other side of the zone center Q=0 illustrate the crystal symmetry in reciprocal space. This symmetry is demonstrated even more convincingly in the Appendix where we experimentally prove the existence of cross correlations across an inverse lattice parameter. The questionable quality of the fits that were used to determine the decay rates is expressed in terms of the quantity $k_2\Gamma^{-2}$ in Fig. 8(b) that involves the second cumulant k_2. Although this figure provides only qualitative information on the presence of more than a single characteristic decay time constant in the time interval of interest, there is a tendency that the fit is poorest for values of Q very close to the zone center and halfway through the first Brillouin zone. We emphasize that the poor quality of the fits is *not* due to the presence of flares of reflected light; all these measurements were done in a heterodyne setup.

The hydrodynamic theory of lattice dynamics predicts the dependence of the relaxation rate Γ of the correlation function on the wave vector Q

$$\Gamma=\frac{1}{6\pi\eta a}(8A_1+8A_2+16B_1/3+4B_2)\sin^2(\pi Q)\times[1-\kappa^L_{110}(Q)\phi^{1/3}]\,, \tag{18}$$

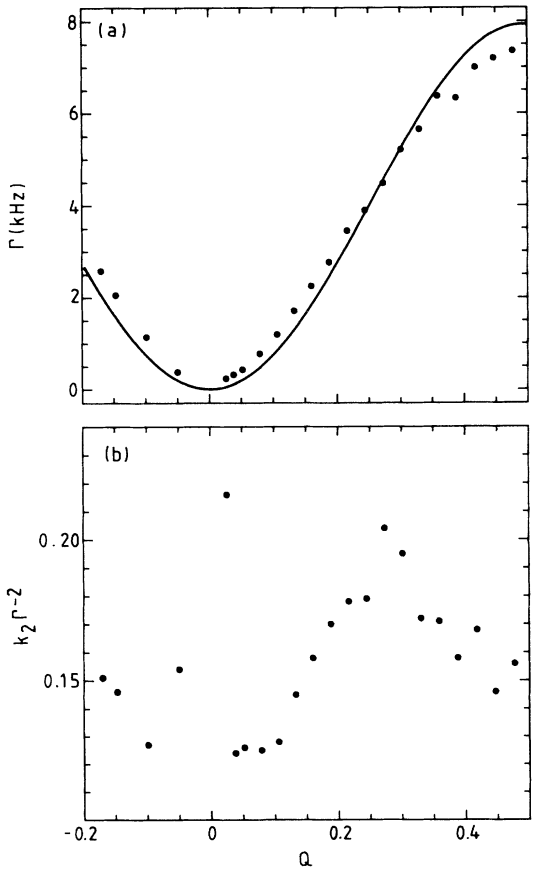

FIG. 8. (a) Dots: measured dispersion function of longitudinal waves in the [110] direction as a function of reduced wave vector $Q=q\sqrt{2}R_0/4\pi$. Line: fit of hydrodynamic theory by adjusting the crystal elastic parameter. (b) Normalized second cumulant of measured heterodyne correlation functions as a function of (reduced) wave vector Q.

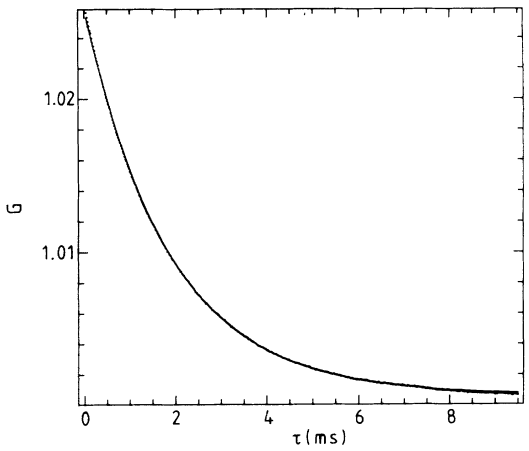

FIG. 9. Dots: measured correlation function G of light scattered by a transverse wave with $Q=0.06$ in the [100] direction. Line: fit of $G=c_1\exp(-\Gamma\tau)+c_2$, with $\Gamma=535$ Hz, $c_1=2.5\times10^{-2}$, and $c_2=1.001$.

where we have used the well-known expression for the elasticity tensor $D(\mathbf{q})$ in a bcc lattice with parameters $A_{1,2}$ and $B_{1,2}$ that characterize potential interactions V with nearest neighbors (A_1,B_1) and next-nearest neighbors (A_2,B_2) in the lattice. These interactions are

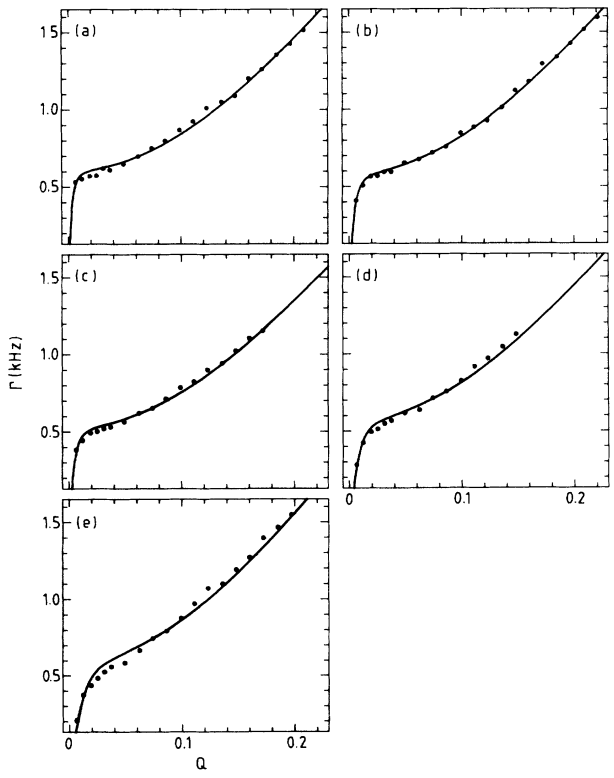

FIG. 10. Dots: measured transverse mode dispersion functions as a function of reduced [100] wave vector $Q=qR_0/4\pi$ for various cell separations $L=128$, 78, 49, 34, and 27 μm in frames (a)–(e), respectively. The corresponding lattice parameters are $R_0=0.74$, 0.76, 0.79, 0.77, and 0.79 μm, respectively. Lines: fit of hydrodynamic theory by adjusting the crystal elastic parameters and the residual zero-wave-vector damping (see text).

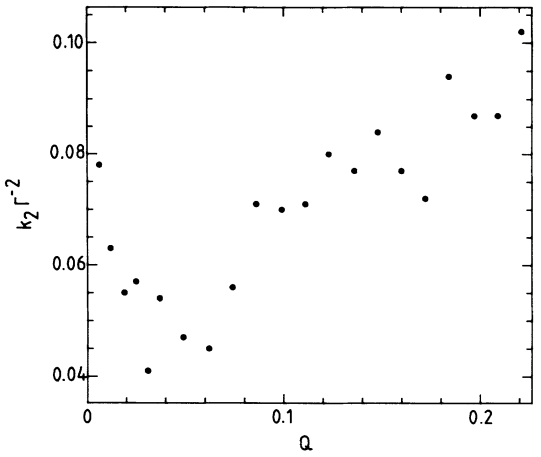

FIG. 11. Normalized second cumulant of measured heterodyne correlation functions of light scattered by transverse waves as a function of wave vector Q at a cell separation of 78 μm [see Fig. 10(b)].

represented as second-order tensors $V=A_1 I+B_1\hat{\mathbf{R}}\hat{\mathbf{R}}$, and similarly for those between next-nearest neighbors involving the constants A_2, B_2. The value of $(8A_1+8A_2+16B_1/3+4B_2)=1.03\times10^{-5}$ N m^{-1} was determined in a least-squares procedure.

Figure 9 shows a transverse correlation function measured from the same crystal and at the same cell separation as the longitudinal curve of Fig. 7. Light was scattered by transverse waves in the [100] direction with reduced wave vector $Q(=qR_0/4\pi)=0.06$. A qualitative but essential observation is that, contrary to the longitudinal case, transverse correlation functions *do* show simple exponential behavior. This is demonstrated by the quality of the fit $G_1^T=c_1+c_2e^{-\Gamma\tau}$ that is also shown in Fig. 9. Therefore transverse correlation functions can be condensed adequately into dispersion functions.

Figure 10 shows a series of dispersion functions of transverse crystal waves for Q values smaller than $Q=0.2$. The crystals were grown from solutions of 0.053 μm radius spheres in deionized water. In order to study the influence of possible wall effects, the cell separation was varied from 128 μm [Fig. 10(a)] to 27 μm [Fig. 10(e)]. Each measured point in Fig. 10 is the decay rate Γ of an exponential fitted to a measured heterodyne correlation function; the fits extended over a time interval $[0,5\Gamma^{-1}]$.

TABLE I. Lattice parameter (R_0), elastic constant (c_1) and residual damping of shear waves ($\eta C(l)/\rho$) as a function of the cell spacing (L) of the crystalline samples that were used to study the effects of boundaries on the dispersion of shear waves (see also Figs. 10, 13, and 14).

L (μm)	R_0 (μm)	$\eta C(l)/\rho$ (kHz)	c_1 (10^{-5} N m^{-1})
128	0.74	2.1	1.8
78	0.76	5.1	1.8
49	0.79	4.6	1.7
34	0.77	13.1	1.8
27	0.79	27.3	1.9

Figure 11 shows the nonexponentiality parameter $k_2\Gamma^{-2}$ as a function of Q for the case shown in Fig. 10(b). Comparison with that of longitudinal correlation functions shows that it is more than a factor of 2 smaller for transverse correlation functions. The adjustment of the cell spacing caused melting of or at least severe damage to the crystals. Therefore all curves in Fig. 10 are from different crystals, each with its own lattice parameter and crystal-elastic constant; these are listed in Table I.

The dramatic influence of the bounding walls of the thin-film cell is clearly demonstrated in Fig. 10. At the largest cell separation (128 μm), the relaxation rate tends to a finite value at the zone center where the damping vanishes as $\lambda_q^T\simeq q^2$. For smaller cell separations L the relaxation rate Γ still apparently tends to a finite value for decreasing Q, but for $Q<Q_0$ sharply drops to zero. It appears that the value of Q_0 is of the order of the smallest possible wave number in a direction perpendicular to the cell walls $Q=R_0/2L\cong10^{-2}$. Incidentally we notice that our scattering vectors are parallel to the glass surfaces of the cell so that the sharpness of Bragg reflections and the definition of the wave vector Q does not depend

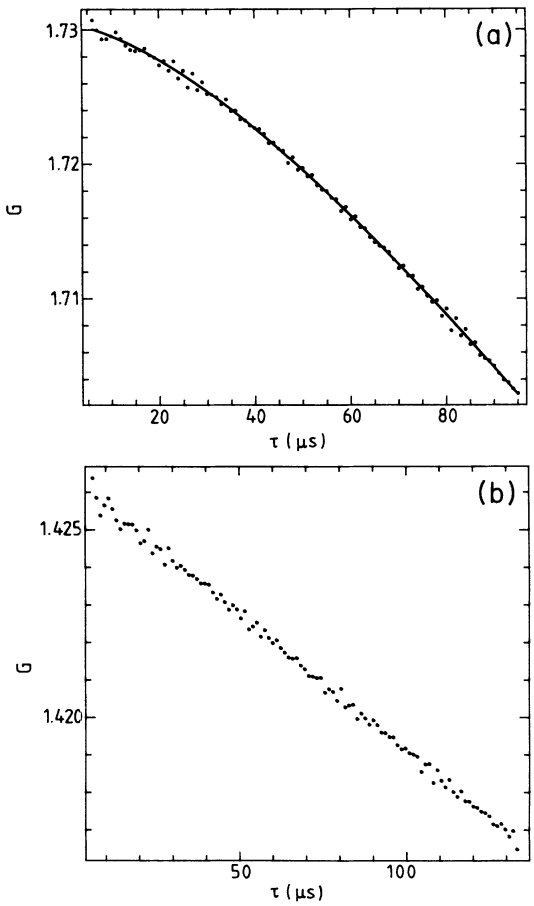

FIG. 12. Homodyne correlation functions of long-wavelength phonons. (a) Dots: transverse mode with $Q=0.0062$ in the [100] direction. Line: fit of $G=c_1-\Gamma_1\tau-c_2\exp(-\Gamma_2\tau)$ with $c_1=1.75$, $c_2=0.016$, $\Gamma_1=4.4\times10^2$ s^{-1}, and $\Gamma_2=2.3\times10^4$ s^{-1}. (b) Longitudinal mode correlation function with $Q=0.013$ in the [110] direction.

on the cell separation.

So far, our experimental results were for the smallest of the characteristic frequencies of longitudinal and transverse modes that were introduced in Sec. II as ω_2^L and ω_3^T, respectively. However, for transverse waves the hydrodynamic theory predicts the existence of a relaxation time $1/|\omega_2^T|$ that is intermediate between the slowest time scale for these waves and the fast relaxation time of the Brownian velocity autocorrelation. This intermediate time scale is in the long-wavelength limit associated with the relaxation of pure hydrodynamic shear modes, $\omega_2^T = i\eta q^2/\rho$.

Figure 12 shows small-time correlation functions of light scattered by very long transverse and longitudinal waves. The curves were measured in a homodyne scattering setup that offered a slightly better signal-to-noise ratio. It was checked, however, that the results were in accord with a heterodyne measurement. The crystal parameters were $a = 0.053$ μm, $R_0 = 0.67$ μm, and the cell separation $L = 31$ μm. Longitudinal waves were with $Q = 0.013$ in the [110] direction; transverse waves had $Q = 0.0062$ in the [100] direction. The overall downward slope of the correlation functions is on the slowest time scale, $1/2|\omega_2^L|$ and $1/2|\omega_3^T|$ for longitudinal and transverse waves, respectively. For $\tau < 40$ μs the transverse correlation function has a negative exponential contribution that is absent in the longitudinal correlation function. This observation is in perfect agreement with the theory sketched in Sec. II. In order to extract the relaxation rate Γ_2 of this swiftly decaying component, we represented measured transverse correlation functions by $G(\tau) = c_1 - \Gamma_1\tau - c_2\exp(-\Gamma_2\tau)$, and determined Γ_2 in a least-squares procedure. Figure 13 shows the relaxation rate Γ_2 as a function of $\eta q^2/\rho$. The theoretical prediction is that the relaxation of long-wavelength shear waves should equal that of pure hydrodynamic shear waves, $\Gamma = \eta q^2/\rho$. Figure 13 also contains points that were deduced from the small-Q part of the transverse dispersion curves of Figs. 10(d) and 10(e) using elastic constants that were deduced from their large-Q parts.

A remarkable conclusion is that the measured relaxation rates approximately follow those of hydrodynamic shear modes in an infinite medium, but are shifted upwards by approximately 30 kHz at this thin-film thickness. Another qualitative but important observation is that longitudinal correlation functions do *not* show the presence of an intermediate time scale [$O(10^{-5}$ s)]. As argued in Sec. II, the presence of such a time scale would be expected on the basis of electrodynamic effects related

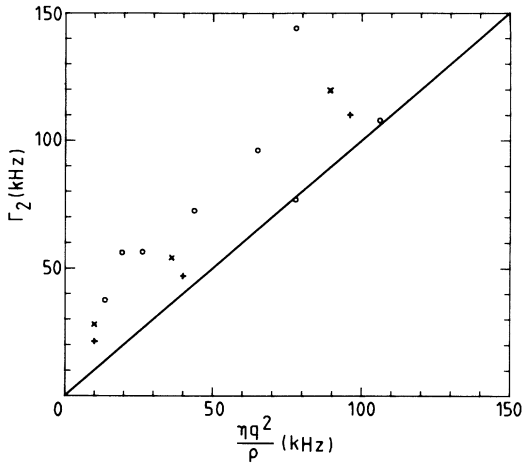

FIG. 13. Dots: measured dispersion function of the shear relaxation $\Gamma_2 = i\omega_2^T$ as a function of $\eta q^2/\rho$ at a cell separation of $L = 27$ μm. Line: $\Gamma_2 = \eta q^2/\rho$. Crosses and plusses: λ_q^T/μ_q^T deduced from Figs. 10(d) and 10(e), respectively (see text).

to ion diffusion, effects that would be strongest in the case of longitudinal waves where the relative motion of fluid and spheres is largest. In this respect, the absence of structure on the smallest measured time scale in Fig. 12(b) sets an upper bound on the Debye length κ^{-1} in our samples, $\kappa R_0 > 2$.

Figure 13 suggests that the damping λ of shear waves in a crystal of finite thickness L can be parametrized by $\lambda = (\eta/\rho)[q^2 + C(L)]$. The following simple argument shows that such behavior may be explained by the discreteness of the hydrodynamic mode structure in a narrow slit. This discreteness owes to the necessary satisfaction of no-slip boundary conditions at the cell surfaces, $z = 0, L$. Fluctuations of the fluid velocity field have therefore the structure

$$\tilde{v}_n(q_x, q_y, t) \cong e^{i(q_x x + q_y y)} \sin(n\pi z/L) \times e^{-(\eta/\rho)(q_x^2 + q_y^2 + n^2\pi^2/L^2)t} . \tag{19}$$

In our experiment $\mathbf{q}$ is parallel to the cell surface and Eq. (19) implies that a finite relaxation rate $\eta n^2\pi^2/\rho L^2$ remains at $q = 0$, so that $C(L) = c/L^2$. The finite residual damping of shear phonons also determines the shape of the dispersion functions of the complementary slow mode $\omega_3^T = -i(\omega_q^T)^2/\lambda_q^T$ shown in Fig. 10. Use of the known form of the crystal elasticity $D(\mathbf{q} = [100])$ then predicts for this relaxation rate

$$\omega_3^T = -i\{(8A_1 + B_1/3)[1 - \cos(2\pi Q)] + 4A_2\sin^2(2\pi Q)\} \frac{1}{6\pi\eta a} \left\{ 1 - \kappa_{110}^T(Q)\phi^{1/3} + \frac{3a}{4\pi R_0(Q^2 + R_0^2 C(L)/16\pi^2)} \right\} . \tag{20}$$

This expression has been used to represent our data measured in a range of cell separations that are shown in Fig. 10. The constants $c_1 = 8A_1 + B_1/3$ (nearest-neighbor interaction) and $C(L)$ were determined in a least-squares procedure, the constant involving next-near-neighbor interaction turned out to be much smaller than c_1 and was put to zero in the fit. The fair quality of the fits is demonstrated in Fig. 10; the constants used are listed in Table I. The residual damping at infinite wavelength $\eta C(L)/\rho$ is shown as a function of L^{-2} in Fig. 14. The measured

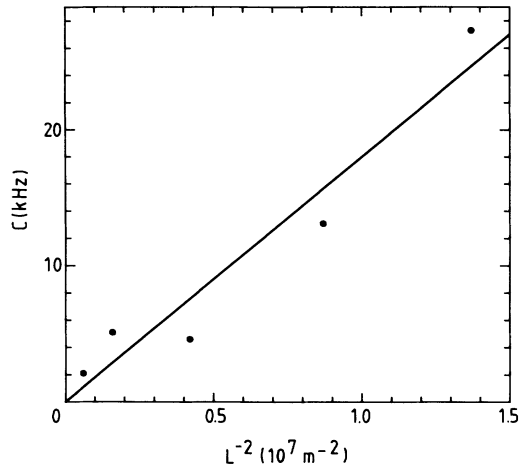

FIG. 14. Dots: the residual damping $C(L)$ of zero-wave vector transverse waves in the [100] direction as a function of L^{-2}, where L is the cell separation.

dependence is indeed consistent with the predicted $C(L)=cL^{-2}$, however, the measured proportionality constant is about a factor of 2 larger than that predicted by Eq. (22) with $n=1$, the first nontrivial transverse mode. A possible explanation for this discrepancy is that the damping of waves polarized parallel to the cell walls is not just that of pure hydrodynamic shear modes, but is influenced partly by hydrodynamic interaction between the wall and the lattice of spheres.

V. CONCLUSION

Our experiments have shown that the damping of shear modes remains finite in the long-wavelength limit because of the finite separation of the cell walls. A tentative theory involving the discreteness of the hydrodynamic mode structure has been proposed and we speculate that the behavior of shear modes can be understood solely in terms of hydrodynamics. This leaves us with profound questions about the relevance of electrodynamic effects associated with the motion of counterions. The theory by Felderhof and Jones [6] that is sketched in Sec. II states that one needs these electrodynamic effects to explain the finite damping of long shear waves.

We speculate that electrodynamic effects are responsible for the nonexponential behavior of measured correlation functions of light scattered by longitudinal modes. This nonexponentiality is another significant result of our work. It has been noticed earlier by Hurd *et al.* [3], who attribute it to the presence of a heterodyne component of the correlation function, to possible multiphonon processes, and to memory effects in the dynamics of shear modes. The first of these explanations can now be ruled out: explicit heterodyne measurements of longitudinal waves remain nonexponential, whereas heterodyne correlation functions of light scattered by transverse modes are characterized by single-exponential decay. It further is hard to imagine why longitudinal modes would be affected more strongly by anharmonicity (multiphonon) effects than transverse modes.

The nonexponentiality of longitudinal correlation functions is apparently not implied by a theory of electrodynamic effects based on diffusive counterion dynamics alone [6]. Neither has the presence of an ion-diffusion time scale been observed in our experiment. However, we have not yet probed fast enough time scales. As was already suggested by Felderhof and Jones, we believe a complete theory should also account for electrophoretic effects: the convection of counterions by flowing solvent fluid. Further work with samples whose electrical properties can be characterized precisely *in situ* is clearly needed to resolve the discrepancies between the theory of

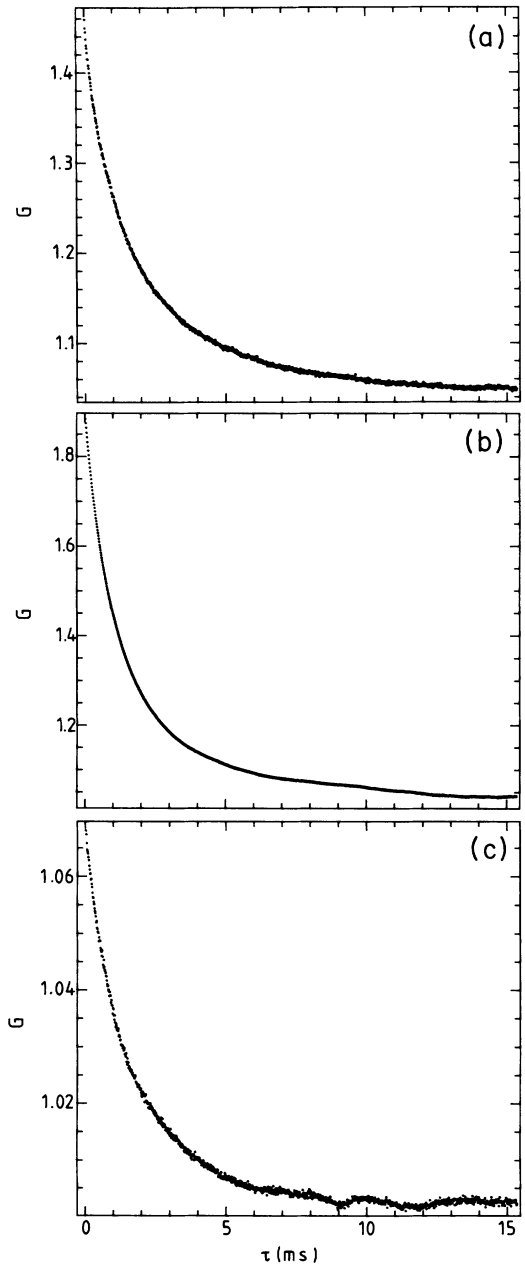

FIG. 15. (a) Measured homodyne autocorrelation function at $\theta_1=2.5°$. (b) Homodyne autocorrelation function at $\theta_2=80.5°$. (c) Measured homodyne cross-correlation function between the detectors at $\theta_1=2.5°$ and $\theta_2=80.5°$.

electrical interactions and experiment. For this, a novel design of the scattering cell is needed.

The possibility of thermally driven underdamped shear modes remains an intriguing aspect of the dynamics of colloidal crystals. These modes would give rise to oscillatory correlation functions. We have shown that, so far, they have remained unobserved because of the finite thickness of the thin-film samples used. The numbers extracted from the results displayed in Figs. 10 and 13 suggest that in our samples propagating modes would occur first at $Q=0.75\times10^{-3}$, and a cell separation of $L=0.35$ mm.

We finally notice that information on hydrodynamic shear modes would be very hard to come by in isotropic fluids [19]. In colloidal crystals the lattice of spheres acts as a tracer that in the long-wavelength limit faithfully follows the flow.

ACKNOWLEDGMENTS

This work is part of the research program of the "Stichting voor Fundamenteel Onderzoek der Materie (FOM)" which is financially supported by the "Nederlandse Organisatie voor Wetenschappelijk Onderzoek (NWO)." The authors are deeply indebted to Dr. Brigitte Pansu, who introduced them to methods of sample preparation and they thank Jan Niessen for technical assistance and Professor P. P. J. M. Schram for helpful discussions.

APPENDIX: CROSS CORRELATIONS IN COLLOIDAL CRYSTALS

Due to crystal symmetry a single phonon scatters light in directions that have translation symmetry in reciprocal space. This is expressed by the symmetry of measured dispersion functions around zone centers and zone boundaries (See Fig. 8). While this symmetry is that of a *time-averaged* quantity, it should also apply to the *instantaneous* scattered light intensity. Specifically, the fluctuations measured in two points that are separated by an inverse lattice distance should be in phase [20]. In this appendix we will experimentally demonstrate the existence of cross correlations between the intensity detected at these two points. While the existence of these cross correlations may be trivial in theory, its actual verification in the experiment is a strong justification of the experimental techniques used.

The study of fluctuations in colloidal crystals by scattering visible light is analogous to the technique of neutron or x-ray scattering off atomic crystals. In fact, the analysis of fluctuations by correlation functions as sketched in Sec. II dates back to the early papers by Wang and Uhlenbeck [21]. Proving the existence of similar cross correlations in experiments on atomic crystals is elusive, but can quite easily be done for visible light scattered by colloidal crystals.

In the scattering experiment, two separate detectors detect light with scattering vectors $\mathbf{k}_1$ and $\mathbf{k}_2$. The cross-correlation function of the scattered electric field is, in analogy with Eq. (14)

$$g_1(\mathbf{k}_1,\mathbf{k}_2,\tau)\simeq \sum_{l_1,l_2}\sum_{q} P_1^*(\mathbf{k}_1-\mathbf{q}-\mathbf{K}_{l_1})P_2(\mathbf{k}_2-\mathbf{q}-\mathbf{K}_{l_2})\sum_{\beta}\mathbf{k}_1^{\beta}\mathbf{k}_2^{\beta}\rho_q^{\beta}(\tau)\ , \tag{A1}$$

where $P_1(\mathbf{k})$ is the profile function of the scattering volume that is observed by the first detector and $P_2(\mathbf{k})$ is the profile function of the second detector. The condition for observing cross correlations is that $\mathbf{k}_1-\mathbf{k}_2\cong\mathbf{K}_{l_1}-\mathbf{K}_{l_2}$, within the uncertainty set by the profile functions P_1 and P_2. The width Δk of these functions is inversely proportional to the linear size d of the scattering volume. Therefore the detectors have to be aligned with a scattering angle accuracy $\Delta\theta\cong\lambda/2\pi d$. In our setup angles can be adjusted to 0.2°, therefore d has to be approximately 30 μm.

The two detectors were separated precisely by an inverse lattice distance by rotating the crystal such that one detector accepted Bragg-reflected light, whereas the other one was placed in the incident beam. Next the cell and the two detectors were rotated over an angle θ_1 around a vertical axis and a homodyne cross-correlation function is measured.

The experiment was done on a $L=31$ μm thick crystal of 0.053 μm polystyrene spheres with lattice parameter $R_0=0.71$ μm. The incident beam was focused in the cell to a diameter of 40 μm. For practical reasons the scattering angle θ_1 was restricted to small values. Figure 15 shows two homodyne autocorrelation functions measured for detector 1 and 2 and their cross-correlation function. The contrast in the measurement using the detector that is closest to the incident beam direction is lower than that from detector 2 that is placed at $\mathbf{k}_2=\mathbf{k}_1+\mathbf{K}_{110}$. This is most probably due to partial heterodyning at detector 1 due to stray light from the incident beam and is consistent with the slight differences in the decay time scales of the three correlation functions. The low contrast of the cross-correlation function must be caused by a slight mismatch in the difference of scattering vectors with respect to $\mathbf{K}_{110}$.

[1] P. Pieranski, Contemp. Phys. **24**, 25 (1983).
[2] H. Hasimoto, J. Fluid Mech. **5**, 317 (1959).
[3] A. J. Hurd, N. A. Clark, R. C. Mockler, and W. J. O'Sullivan, Phys. Rev. A **26**, 2869 (1982).
[4] A. J. Hurd, N. A. Clark, R. C. Mockler. and W. J. O'Sullivan, J. Fluid Mech. **153**, 401 (1985).
[5] B. U. Felderhof and R. B. Jones, Z. Phys. B **64**, 393 (1986).
[6] B. U. Felderhof and R. B. Jones, Faraday Discuss. Chem. Soc. **83**, 69 (1987).
[7] D. H. van Winkle and C. A. Murray, Phys. Rev. A **34**, 562 (1986).
[8] B. J. Ackerson and N. A. Clark, Physica A **118**, 221 (1983).
[9] N. A. Clark, B. J. Ackerson, and A. J. Hurd, Phys. Rev. Lett. **50**, 1459 (1983).
[10] See, for example, H. M. Lindsay and P. M. Chaikin, J. Chem. Phys. **76**, 3774 (1982); T. Okubo, *ibid.* **87**, 6733 (1987).
[11] J. Happel and H. Brenner, *Low Reynolds Number Hydrodynamics,* 2nd ed. (Noordhoff, Leiden, 1973).
[12] J. M. Burgers, *2nd Report on Viscosity and Plasticity* (Koninklÿke Nederlandse Akademie van Wetenschappen, Amsterdam, 1938).
[13] C. Kittel, *Introduction to Solid State Physics,* 4th ed. (Wiley, New York, 1971).
[14] J. G. McWhirter and E. R. Pike, J. Phys. A **11**, 1729 (1978).
[15] E. Jakeman, in *Photon Correlation and Light Beating Spectroscopy,* edited by H. Z. Cummins and E. R. Pike (Plenum, New York, 1974).
[16] P. N. Pusey and W. van Megen, Physica A **157**, 705 (1989). Their treament of light scattering by nonergodic media finds a direct but maybe trivial application in the case of colloidal crystals. A crucial element of this application is, contrary to amorphous media, the absence of static light scattered outside Bragg reflections in colloidal crystals.
[17] By using a cross-correlation technique, pure transverse waves can be detected with wave vectors restricted to $\mathbf{q}=\mathbf{K}_l/2$.
[18] A theory for the reduction of the sedimentation velocity of charged spheres due to ionic friction has been described by H. Ohshima, T. W. Healy, and L. R. White, J. Chem. Soc. Faraday Trans. 2 **79**, 1613 (1983). Their result is in the form of an analytic expression containing integrals that were computed numerically. For low ζ potentials they have approximated their results in terms of transcendental functions with argument κa. Equation (17) is the first-order expansion (in κa) of the latter result. In our case we estimate $\kappa a \cong 0.14$ and the reduced ζ potential $e\zeta/k_B T \cong 10$, which justifies both approximations to the theory of Ohshima, Healy, and White. Similar experiments on the diffusion of charged colloidal spheres have been reported by G. A. Schumacher and T. G. M. van de Ven, Faraday Discuss. Chem. Soc. **83**, 75 (1987). Incidentally we notice that their Fig. 1 is in error.
[19] J. P. Boon and S. Yip, *Molecular Hydrodynamics* (McGraw-Hill, New York, 1980).
[20] The corresponding antiphase fluctuations at opposite inverse lattice points can only be observed either in a heterodyne cross-correlation experiment, or in situations where the scattered light is strongly non-Gaussian.
[21] M. C. Wang and G. E. Uhlenbeck, Rev. Mod. Phys. **17**, 323 (1945).